Published in final edited form as:
Colloids Surf B Biointerfaces. 2011 January 1; 82(1): 173–181. doi:10.1016/j.colsurfb.2010.08.031.

Surface Oxide Net Charge of a Titanium Alloy; Comparison Between Effects of Treatment With Heat or Radiofrequency Plasma Glow Discharge

Daniel E. MacDonald[a,b,c,*], **Bruce E. Rapuano**[a], and **Hannes C. Schniepp**[d]

[a] Hospital for Special Surgery affiliated with the Weill Medical College of Cornell University, 535 East 70th Street, New York, NY 10021, USA

[b] General Medical Research, James J. Peters VA Medical Center, 130 West Kingsbridge Road, Bronx, NY, 10468, USA

[c] Langmuir Center for Colloids and Interfaces, Columbia University, 911 S.W. Mudd Building, Mail Code 4711, 500 West 120th Street, New York, NY 10027, USA

[d] The College of William and Mary, Department of Applied Science, Williamsburg, VA 23185, USA

Abstract

In the current study, we have compared the effects of heat and radiofrequency plasma glow discharge (RFGD) treatment of a Ti6Al4V alloy on the physico-chemical properties of the alloy's surface oxide. Titanium alloy (Ti6Al4V) disks were passivated alone, heated to 600 °C, or RFGD plasma treated in pure oxygen. RFGD treatment did not alter the roughness, topography, elemental composition or thickness of the alloy's surface oxide layer. In contrast, heat treatment altered oxide topography by creating a pattern of oxide elevations approximately 50–100 nm in diameter. These nanostructures exhibited a three-fold increase in roughness compared to untreated surfaces when RMS roughness was calculated after applying a spatial high-pass filter with a 200 nm cutoff wavelength. Heat treatment also produced a surface enrichment in aluminum and vanadium oxides. Both RFGD and heat treatment produced similar increases in oxide wettability. Atomic force microscopy (AFM) measurements of metal surface oxide net charge signified by a long range force of attraction to or repulsion from a (negatively charged) silicon nitride AFM probe were also obtained for all three experimental groups. Force measurements showed that the RFGD-treated Ti6Al4V samples demonstrated a higher net positive surface charge at pH values below 6 and a higher net negative surface charge at physiological pH (pH values between 7 and 8) compared to control and heat-treated samples These findings suggest that RFGD treatment of metallic implant materials can be used to study the role of negatively charged surface oxide functional groups in protein bioactivity, osteogenic cell behavior and osseointegration independently of oxide topography.

Keywords

titanium alloy; oxides; surface treatments; net surface charge; wettability

[*]Corresponding author: Tel.: 212-606-1445; Fax: +1-212-774-7877, dem14@columbia.edu.

1. Introduction

The optimal osseointegration of metallic prosthetic implants employed in the fields of orthopedics and dentistry ultimately depends on the material being used and the surface characteristics of the material. There are a few biomaterials in wide use today that exhibit osseointegratibility. Titanium and titanium alloys are widely employed in orthopedics and dental implants due to their biocompatibility [1,2]. In the dental field, commercially pure titanium (cpTi) and a titanium alloy (Ti6Al4V) have been successfully utilized [3]. Titanium is characterized by different degrees of purity and mechanical properties. The biocompatibility of titanium is due to a thin, retentive oxide film covering and protecting the underlying metal from corrosion. The protective effects of the oxide layer against corrosion can prevent the release of toxic metal particles which can evoke an osteolytic reaction that leads to implant loosening and failure. Nevertheless, a significant percentage of implants do fail anyway, with aseptic loosening as a leading cause of 90% of total hip arthroplasty failures in the U.S. and other countries [4–5]. Despite the reported long-term predictability of dental implants [6–7], failures also occur in 10% of cases within a 5-year period [8]. The process of aseptic loosening is related to both osteolysis and mechanical loosening and develops at the interface between the implant and bone. In this process, loosening occurs when the mechanical burden placed on the implant causes interfacial stresses that exceed the interfacial strength between the implant and the surrounding bone. The quality and quantity of bone is generally believed to be one of the major determinants for implant success [9]. Conversely, inadequate osseointegration that is likely associated with poor quality and quantity of bone at the implant interface enhances the vulnerability of the implant to loosening and failure.

Several recent approaches have emphasized the modification of the metallic implant surface's physical and chemical properties in order to enhance protein binding/bioactivity, the attraction of appropriate cell types and implant integration [10–14; see companion paper, 15]. However, relatively few studies have focused on the importance of the metallic implant's surface oxide in bone cell attachment/function and implant integration. Both titanium and Ti6Al4V form a surface oxide layer capable of interacting with biological fluids and cells when implanted in situ [16–18]. We have demonstrated that the heat treatment of a titanium alloy (Ti6Al4V) increased the hydrophilicity of the surface oxide of Ti6Al4V and the attachment of osteogenic cells to adsorbed fibronectin [13]. These findings suggest that the concentration of reactive functional groups or the net charge of the surface oxide was altered by heat treatment, thereby resulting in an enhancement of adsorbed fibronectin's bioactivity. However, since heat treatment also modified other properties of the oxide [13], this method cannot be utilized to identify the critical oxide physico-chemical property that modulates protein adsorption, bioactivity, bone cell attachment/function and implant integration.

Radiofrequency plasma glow discharge (RFGD) treatment has been used to clean, sterilize and chemically alter the surfaces of materials to improve or change cell adhesion properties by using an RF excitation source to create a low-temperature gas plasma [19–21]. Plasma generated from ordinary atmosphere or oxygen gas can be used to implant oxygen anions onto materials, thereby increasing surface oxide concentration [22–23], wettability [23–24] and the number of hydroxyl groups [22,25–26]. Since hydroxyls complexed with titanium or aluminum have an isoelectric point at a pH of 4.7–6.2 and 3.5 [27], respectively, these functional groups are likely to be negatively charged when exposed to an aqueous environment at pH 7.4. Therefore, our objective was to show whether RFGD could be used to increase the metal oxide surface's net charge, especially at physiological pH, without introducing other complicating factors such as changes in oxide elemental composition and a transformation in the oxide's surface topography. The investigation of the potential relationship between treatment-induced increases in the oxide's surface net charge and an enhancement in adsorbed fibronectin's cell binding activity is presented in our companion article [15].

2. Materials and Methods

2.1 Materials

RBS 35® detergent was obtained from Fisher Scientific Inc. (Rockford, IL). All other chemicals were from Sigma-Aldrich (St. Louis, MO) and were of spectroscopic grade.

Cylindrical implant disks were engineered to a 2-degree taper to enable the disks to form a tight seal when inserted into the well of a 96-well cell culture plate. These disks were initially prepared from Ti6Al4V sheets obtained from TIMET (Wentzville, MO) that were cut into strips and later punched into disks (Industrial Tool & Die Co., Troy, NY). The strips were initially prepared with 240 and 320 grit aluminum oxide abrasive belts, followed by polishing with finer grit polishing compounds on a series of buff wheels to a high luster, and cleaned using a trichloroethylene vapor degreaser (Williams Metal Finishing, Inc., Sinking Spring, PA). The Ti6Al4V disks (8 mm diameter/1.0 mm thick) were then fabricated by running the polished strips through a specially designed punch press and deburred manually on a custom vacuum apparatus (MacDonald, in preparation). This apparatus avoids scratching the highly polished surface through a process in which the metal strips are punched into disks by cutting through the unpolished side and the disks are extracted using Teflon coated die plunger, transported through Teflon tubes, and collected in a padded tray.

2.2 Disk Preparation

2.2.1 Controls—Disks were washed successively in isopropanol, acetone, xylene, acetone, and 1 M ammonium hydroxide, 40% nitric acid, and rinsed with deionized water according to the ASTM-F86 protocol [28]. The disks were then passivated, dried, sterilized and stored as previously described [13].

2.2.2. Heat and RFGD Treatment—The alloy disks were heated to a temperature of 600 °C in air as previously described [13]. RFGD plasma treatment of disks was performed using a modified Harrick RF unit (Ossining, N.Y.) (PDC-002) with a quartz chamber to subject samples to an oxygen plasma treatment. Ti6Al4V disks were passivated as previously described [13] to form a stable surface oxide layer [29] and placed on a clean quartz tray. The tray was inserted into the RF unit and the unit was placed under dry vacuum (EcoDry-M oil-less vacuum pump; Leybold Vakuum, Köln, Germany). When the vacuum was low enough (1600 mTorr) to remove all water vapor, oxygen was gradually bled into the system via a needle valve. The gas flow rate was monitored using an Omega shielded flow meter (Omega Technologies Co, Stamford, CT) at a rate of 250 ml/minute. All oxygen gas was prefiltered prior to its entry into the chamber (Advantec MFS, Inc, Pleasanton, CA). Samples of titanium alloy were treated with a 13.56 MHz RF power-generated oxygen plasma for 5 min at 29.6 W. Following heat or RFGD treatment, disks were sterilized and stored as previously described for untreated (control) specimens [13].

2.3. Surface analysis

2.3.1. Atomic Force Microscopy Imaging for Roughness Analysis—Atomic Force Microscopy (AFM) was used to image untreated control and treated alloy disk surfaces to determine their surface topography. Our NTEGRA Prima Scanning Probe Laboratory (NT-MDT, Zelenograd, Russia) was employed in tapping mode under ambient conditions. The probes were rectangular NSG-01 silicon levers with an aluminum back coating (NT-MDT, nominal values for spring constant k = 5.1 N/m, radius of curvature r = 10 nm, and resonance frequency f_0 = 150 kHz). Several random 1×1 μm, 10×10 μm and 30×30 μm areas on two disks were scanned for each of the control and modified disks.

2.3.2. Electron spectroscopy for chemical analysis—Electron spectroscopy for chemical analyses (ESCA) were used for determination of surface composition and elemental oxidation of both the treated and untreated titanium alloy samples as previously described [30,13]. ESCA analyses were conducted using a Physical Electronics (PHI) model 5600 ESCA spectrometer (Chanhassen, MN), employing a monochromatic X-ray source, Al Kα = operated in the focused spot mode. To determine the elements present on the alloy surfaces, ESCA survey spectra were obtained at an analyzer pass energy of 187.85 eV. For quantification purposes, high-resolution spectra of the elements detected were obtained at a pass energy of 11.75 eV. An 0.8 mm diameter spot size was used for analysis. The atomic percentages of the elements present on the disk surfaces were calculated using software and atomic sensitivity factors included with the instrument data system. The binding energies of ESCA peaks were referenced to C 1s at 284.8 eV.

2.3.3. Wettability properties—The wettability of the control and modified disks was determined using a sessile water drop method measuring contact angle (degrees) as previously described [13].

2.3.4. Atomic force measurements of metal oxide net surface charge in water—All force curves were acquired in picopure water (Millipore Synergy, Millipore Corporation, Billerica, MA.) with a resistivity of 18.2 MΩ cm that had equilibrated at pH 5.6 for 20 minutes (Oakton pH/CON benchtop pH meter, Oakton Instruments, Vernon Hills, IL.). No salts, acids or bases were added to the water. Force spectroscopy was performed using the NTEGRA Prima Scanning Probe Laboratory. The SMENA scan head (tip-scanning configuration, 100×100×10 μm scan range with closed-loop capability for highest positioning accuracy) was applied in conjunction with a closed 4 ml liquid cell containing an inlet and drainage port. We used SiNi probes (BudgetSensors, Sofia, Bulgaria) featuring gold coated, triangular silicon nitride cantilevers; nominal numbers for spring constant, resonance frequency, and tip radius of curvature are k = 0.06 N/m, f = 10 kHz, and r < 15 nm, respectively.

Prior to use, the liquid cell and all components were first cleaned by sonication in Contrad 70 lab detergent (Decon Labs, King of Prussia, Pennsylvania) and thoroughly rinsed in picopure water. The components were further cleaned by a subsequent sonication cycle in methanol, followed by another thorough rinse cycle in picopure water.

Force curves had a total approach/retract range of 400 nm and were acquired at a velocity of 200 nm/s. The raw force data (“force-vs-displacement curves”) was subsequently converted into curves showing the force as a function of true tip–sample distance [31]. To exclude possible effects due to the tip shape and tip contamination, a complete series of measurements on the control and on each of the treated alloy surfaces were conducted using one and the same AFM probe. Therefore, all observed differences in the measured curves are due to actual differences in the sample. On each sample, 30–40 force curves were acquired at 15 different sample locations to exclude effects of sample inhomogeneity and sample contamination. To assure reproducibility of the results, this series of experiments was repeated using a second probe and second batch of alloy samples.

2.3.5. Atomic force measurements of metal oxide net surface charge in buffer—Atomic force spectroscopy was carried out on Ti6Al4V control and treated disks using the same experimental setup as described in section 2.3.5, except that NT-MDT CSG01A aluminum-coated silicon probes with rectangular cantilevers (spring constant 0.03 N/m and tip radius of 10 nm) were used. Sodium nitrate buffers were titrated using prepared sodium nitrate and sodium hydroxide or nitric acid stock solutions to a pH of 3, 4, 5, 6, 6.4, 7, 7.4 and 8. For these buffers, an ionic strength of 2 mM was chosen in order to make the Debye length about 7 nm, long enough that the corresponding electrostatic forces can be discriminated from

the shorter-ranged van der Waals forces in the force curves. Since the isoelectric point (IEP) of silicon is significantly below 3, the AFM probe is negative throughout the pH range of 3–8 investigated here. This enables us to accurately determine the IEP of the titanium surfaces in this pH range.

The AFM silicon probe tip was allowed to reach equilibrium (30 min–1 hour) in buffer and force curves were measured. After each experiment at a given pH value, a small amount of the buffer solution was extracted from the liquid cell to measure its pH value. The deviation between the pH values measured before and after the experiment was typically < 0.1 pH units, within the accuracy of the pH meter. The pH can thus be considered constant for the duration of the experiment. In order to carry out an experiment at a new pH value, 60 ml of buffer at the new pH was flushed through the cell.

The force curves with a total scan range of 200 nm were acquired at an approach/retract rate of 50 nm/s. The starting positions for the force measurements were chosen 170 nm above the sample such that the cantilever was deflected by about 30 nm after establishing contact. A total of three control and treatment disks were analyzed. Five random sample locations per disk were investigated at each pH value and 10 force curves were performed at each site. For a given sample, measurements at all pH values were carried out with one and the same tip in order to exclude systematic force differences due to tip shape.

The force data was analyzed as follows. Line fits to the constant-compliance regime of the approach curves and the zero-force regime (at large tip separations) were carried out. This enabled us to convert the raw curves (force-vs-displacement) into force-vs-distance curves [31]. Force curves with random events or unclean baseline were disregarded. In order to determine the electrostatic forces due to sample surface charges, forces at tip separations < 10 nm were not considered, as van der Waals forces are usually significant at such small distances. For the remaining data points with z > 10 nm electrostatic interactions are the only significant forces. To reduce noise and to obtain representative data, all force curves taken at a particular location of a sample were averaged. Correspondingly, exponential decay curves $f(z) = b \cdot \exp[-a \cdot z]$ were fitted to model the electrostatic double layer forces. The fit parameters a and b represent the Debye length and the hypothetical electrostatic force at zero distance, respectively. We use *b* as a measure for the strength of the electrostatic interaction between the tip and the surface; it represents the product of the surface charge densities at the tip and at the surface for a given tip geometry.

2.4. Statistical analysis

All of the experimental data were summarized and analyzed using a one-way analysis of variance (ANOVA) for all surfaces. The alpha level was set at the 0.05 level.

3. Results

3.1. Surface analysis

The surface topographies of modified and unmodified disks were analyzed using AFM (Figure 1). The control disks showed significant topography, with peak-to-peak ranges of typically 200 nm in a 10×10 μm scan area (see Figure 1A). Virtually all this topography is due to machining and polishing: parallel, linear grooves with micron and submicron feature sizes (Figure 1A). AFM revealed that disks exposed to RFGD oxygen plasma exhibited a surface topography (Figure 1B) that was identical to that of control disks (Figures 1A and 1B). In contrast, heat-treated surfaces imaged by AFM exhibited finer scale surface structure (Figure 1C), compared to the polished samples (Figure 1A), that consisted of numerous oxide projections in each square μm of the disk surface. The number of oxide elevations per square μm of the heated

surface, their dimensions and the remarkable difference in topography between the preheated and either the control or RFGD-treated disks became even more evident at a 1 × 1 μm scan area (Figures 1D-F). Heat treatment created oxide elevations roughly 50–100 nm in diameter (Figure 1F). Neither the unmodified (Figure 1D) nor the RFGD-treated (Figure 1E) surfaces exhibited this (or any other) form of oxide nanostructure.

While the specific topographic differences introduced by heating are obvious to the observer, we also wanted to introduce an objective metric to quantify them. A simple roughness evaluation is not suited for this purpose. The small 50–100 nm elevations created by heating have relatively low heights compared to the pre-existing surface topography of our samples of the alloy due to machining and polishing. Consequently, a simple RMS roughness analysis is not sensitive to small changes in roughness. In order to overcome this difficulty, we first applied a spatial high-pass filter to the measured topography data before we carried out the RMS roughness analysis.

Fast Fourier Transforms (FFT) of the topography $f(x,y)$ were computed to obtain the matrix $F(\upsilon_x,\upsilon_y)$, representing the complex amplitudes of the plane-wave components $\exp[-2\pi I\cdot(\upsilon_x x + \upsilon_y y)]$ with spatial frequencies υ_x and υ_y. We multiplied F by the transfer function $t(\nu_x, \nu_y)=1-\exp[-\kappa_0^2(\nu_x^2+\nu_y^2)]$, with κ_0 = 200 nm. This introduces a soft cutoff such that structures below 100 nm remain virtually unaltered, structures between 200 nm and 400 nm are attenuated by a factor of (e − 1)/e, whereas feature sizes of 400 nm and above are practically eliminated. This can be seen in Figure 1G, which shows the high-pass filtered version of Figure 1B, representing the RFGD-treated alloy surface. Larger structures are removed (the wider valleys), whereas all the small-scale grooves due to polishing were completely preserved. Similarly, Figure 1H shows the high-pass filtered version of the heat treated sample topography (Figure 1C). This spatial high-pass filter approach allows for the analysis of small heat-induced oxide elevations at small length scales without the interference of larger metallic polishing grooves.

The RMS roughness values of these high-pass filtered images; the results are shown in Table 1. After high-pass filtering, the control samples featured a relatively low roughness of only 4.1 ± 1.1 nm. In stark contrast, we found that the heat treated samples exhibited an RMS roughness of 12.8 ± 1.7 nm due to the 50–100 nm grains introduced through the heating process. For the RFGD treated samples, we observed a roughness of 3.6 ± 0.9 nm which demonstrates that the RFGD treatment does not introduce any statistically significant roughening of the alloy substrates. It should also be noted that the method introduced here is completely independent of the investigated image size: all results for 1×1 μm, 10×10 μm, or 30×30 μm scan sizes and pixel dimensions 256×256, 512×512, or 1024×1024 were statistically equivalent. This further underlines the robustness of this method to detect roughness at small length scales, independently of the imaging parameters.

3.2. Oxide thickness and chemical analysis

We have previously reported that a low intensity metallic Ti peak was observed in the ESCA spectrum of control disks, indicating that a thickness of the oxide film is on the order of 5 nm [13]. In the present study, the heat-treated alloy disk did not exhibit a metallic Ti or Al peak, indicating that the treatment had thickened the surface oxide layer. In fact, the heat treatment produces oxide layers that are too thick to be accurately quantified (using depth profiling) by ESCA, as we have previously reported [13]. In contrast, the control and RFGD-treated samples did manifest metallic Ti and Al peaks, reflecting the presence of both metals beneath the surface oxide layer. Metallic Ti and Al were less than approximately 5% of the total peak energies of all of the metal oxides in the specimens analyzed. Therefore, RFGD does not significantly increase oxide layer thickness as does heat treatment. The surface composition of the disks

determined by ESCA is shown in Table 2. For all the disks, C, O, N, Ti, Al and V were detected. The organic carbon detected by ESCA was present at the same levels on unmodified and modified disks. The surfaces are composed primarily of Ti, with lesser amounts of Al and V. The atomic ratios of the metals for the control and RFGD disks were the same, demonstrating that RFGD treatment did not alter the elemental composition of the alloy's surface oxide layer. In contrast, the heated disks exhibited a marked decrease in Ti, with significant increases in Al and V compared to the control and RFGD disks. This indicates that the heat treatment has enriched the surface of the alloy disks in both Al and V relative to Ti, as we have previously reported [13].

ESCA binding energy data provides information about the chemical states of the metals on the alloy disk surfaces. For control, RFGD and heat-treated samples, the primary Ti $2p^{3/2}$ peak occurred at 458.8 eV. This indicates the presence of Ti in the +4 oxidation state, consistent with the presence of TiO_2 on the surface [32,33]. The primary Al 2p peak for control, RFGD and heat-treated disks occurred at 74.4 eV, consistent with the presence of Al+3 as Al_2O_3 on the surface [34–36]. For the control and RFGD samples a broad V $2p^{3/2}$ peak at about 516 eV was observed. This suggests that V is present in a mixture of lower oxidation states, possibly V_2O_3 and VO_2 [37,38]. Therefore, like the atomic composition data, the ESCA energy binding data also demonstrates a similarity in composition between the control and RFGD-treated surfaces. For the heated alloy disks, two V $2p^{3/2}$ peaks were evident in the spectra at binding energies of 517.5 and 516.4 eV. These peaks reflect the presence of V+5 and V+4 on the disk surface, and suggest the presence of V_2O_5 and VO_2 [63], as we have previously reported [13]. The V_2O_5 and VO_2 were present in approximately an 80:20 ratio.

3.3. Wettability properties

RFGD treatment of the titanium alloy resulted in a surface wettability similar to that of our heated samples (Table 3). Either heating or exposing Ti6Al4V disks to RFGD resulted in a substantial and statistically significant increase in surface wettability (contact angles were reduced to 16.0±2.0° and 17.3±6.0°, respectively) when compared to control samples exhibiting a contact angle of 43.0±5.3°.(Table 3).

3.4. Metal surface oxide net charge

The net surface charge of unmodified and modified Ti6Al4V was measured using atomic force spectroscopy. When exposed to water or a buffer, the surface of the AFM tip acquires a charge. When the tip approaches the sample surface, the tip charge interacts with sample charges. The forces associated with tip deflection away from (repulsive force) or attraction towards (attractive force) a sample surface can be used to estimate the net surface charge. The isoelectric point for silicon nitride, the material used in the AFM probe, varies depending on experimental conditions [39–40]. The AFM tip charge was thus determined by measuring its interaction with a freshly cleaved mica surface in picopure water without electrolytes at pH 5.6. The result is shown as a green curve in Figure 2, in which the observed forces are plotted as a function of the true tip–sample separation. By convention, repulsive forces are represented by positive numbers. For tip–surface separations in the range 15–50 nm, a region where only electrostatic forces are relevant, we observed significant repulsion. Since mica has an isoelectric point of ~3.0, the charge of the mica surface is strongly negative at pH 5.6 [41]. The observed repulsion shows that our silicon nitride AFM tip also has a net negative charge at pH 5.6. At distances <10 nm, the electrostatic repulsion is overridden by short-ranged, attractive van der Waals forces.

Subsequently, we acquired force curves on control, heat-treated and RFGD treated Ti alloy surfaces (black, red, and blue curves in Figure 2, respectively) in the absence of electrolytes. The forces for control and heat-treated samples (black and red curves, respectively) are

indistinguishable within the noise level of our measurements. Both curves show attractive forces in the short range from 0 to 10 nm, and no measurable forces for distances >10 nm. The force curve of the RFGD treated sample (blue) exhibits a very similar shape, although the attractive forces exhibit a significantly longer range, with measurable forces present at distances larger than 10 nm. This observed increase in the range of the attractive forces in the RFGD sample can only be explained by an attractive electrostatic component. Therefore, there is a significant positive net surface charge present on the RFGD treated samples at pH 5.6, whereas the control and heat treated samples only exhibit significant forces in the range of 0–10 nm. Within this range, the forces measured are dominated by van der Waals forces.

Force curves were also acquired for control and treated samples in the presence of sodium nitrate buffer at a range of pH values from 3 to 8.4 (Figure 3). The data presented in Figure 3 shows parameter *b* obtained from fits to the force curves for the three surfaces at various pH values as described in Section 2.3.5. This parameter represents the hypothetical zero-distance electrostatic force between the tip and sample and is used as a measure of the strength of the electrostatic tip–sample interactions. The control, preheated and RFGD-treated samples each displayed an electrostatic force of attraction at a pH of 5 or below (Figure 3). However, force measurements revealed a greater electrostatic force of attraction for RFGD-treated samples compared to control samples over this range of acidic pH values In contrast, heat-treated samples displayed a force of attraction that was equivalent to that of control samples between pH 3 and 5 (Figure 3). These results indicate that only RFGD treatment increased the positive net surface charge of the Ti6Al4V alloy measured at acidic pH values. Interestingly, the force measurements using nitrate buffer showed that control samples possessed a positive net surface charge between pH 5 and 6.4 (Figure 3), despite the fact that these samples tested in water were found to have a nominally neutral net surface charge within this pH range (Figure 3).

In contrast to their force measurement patterns observed at pH 5 or lower, both the RFGD-treated and heat-treated samples exhibited an electrostatic force of repulsion between pH 6 and 8.4 (Figure 3). However, control specimens still manifested an electrostatic force of attraction even at pH 6.4 and only demonstrated an electrostatic force of repulsion at a pH of 7 or higher (Figure 3). These results indicated that all three groups of samples displayed a negative net surface charge at physiological pH (between pH 7 and 8), with RFGD-treated > heat-treated > control samples in the magnitude of this net charge. Both treatments shifted the surface isoelectric point of the titanium alloy from approximately pH 6.7 to 5.4 (Figure 3).

4. Discussion

The basic objective of this study was to compare the effects of heat and RFGD treatments of a titanium alloy on the physical and chemical properties of the alloy's surface oxide. Our underlying goal was to determine whether RFGD treatment could be used to modify only the surface chemistry of the alloy's oxide without altering oxide atomic composition or structure. We have shown that the effects of RFGD and heat treatment on surface oxide properties were qualitatively very different. RFGD treatment did not alter surface topography with respect to control. In contrast, the preheating treatment introduced 50–100 nm-sized oxide elevations which were superimposed on metallic polishing groves that are significantly larger in both lateral size and amplitude (see Figure 1C). Interestingly, none of the polishing grooves remain visible after high-pass filtering (Figure 1H). In contrast, the high-pass filtered image of the RFGD treated surface still shows some small-scale grooves. Therefore, we conclude that these groove-like surface features have been converted into the small 50–100 nm-sized oxide grains during the heat treatment. To more accurately quantify the roughness of these nanostructures, we used an advanced method of roughness evaluation that is based on computing the RMS roughness after applying a 200 nm-cutoff high-pass filter to remove the contribution of polishing grooves (> 200 nm). Using this advanced method of roughness measurement, it was

demonstrated that the heat treated surface was much rougher at small length scales compared to control or RFGD-treated specimens. The heat- treated samples featured a roughness of sub-200 nm features which is about 3 times as high as the corresponding roughness of either control or RFGD samples, which are identical within the precision of measurement. These findings clearly show that only the heat treatment increased the roughness of the Ti6Al4V alloy's surface oxide.

Preheating also substantially increased the elemental composition of the oxide compared to polished controls whereas RFGD failed to do so. Interestingly, both heat and RFGD treatment produced a more hydrophilic surface oxide compared to control samples, although the untreated sample oxide was already relatively hydrophilic (water droplet contact angle < 60 degree).. However, the key finding of our study is that both heat and RFGD treatment of the Ti6Al4V produced a more negatively charged surface oxide of the alloy *at physiological pH* compared to the control oxide. Our findings collectively demonstrate that, of the two surface treatments tested, only RFGD can be utilized to selectively alter surface oxide charge without changing its topography or atomic composition. Therefore, the RFGD treatment of metallic implant materials was used in our companion article to study the role of the oxide's net charge, independently of other oxide properties, in protein bioactivity and osteogenic cell behavior [15].

4.1 RFGD and other plasma treatments

Our finding that a 13.56 MHz RF power-generated oxygen plasma creates a more charged oxide in the Ti6Al4V alloy has not been previously reported. In RFGD, an RF generator provides a high voltage alternating current in the radiowave frequency of the electromagnetic spectrum to create a low temperature plasma in a process gas region. RFGD produces a plasma composed of energetically active species including electrons, free radicals, charged monoatomic species and photons [42]. Other studies have instead employed a direct current-generated glow discharge plasma (GDP) that is produced by a continuous potential difference applied between a cathode and anode located some distance apart in a gaseous medium. A number of studies have employed a GDP using argon gas and measured its effects on titanium surface hydrophilicity [69], the elimination of surface contaminants [43] and bone cell attachment [44]. There are a number of considerations suggesting that RF oxygen plasma and DC argon plasma will have different effects on the physical, chemical and biological properties of the oxide.

Differences between the DC current and RF plasma treatment of titanium materials in their effects on surface oxide properties, protein adsorption/bioactivity and bone cell behavior (see ref.15) may occur as they produce plasmas with different properties. In our study, an AC current generated oxygen plasma created by RFGD is likely to implant different particles compared to a GDP+ argon plasma, which exclusively induces the accumulation of electrons at one electrode, the powered anode.{45]. In contrast, RFGD plasmas are likely to implant positive ions, neutral species as well as electrons, since the AC current periodically reverses voltage polarity at each electrode. Another consideration is that DC-glow discharge forms different regions (e.g. dark space, negative glow, positive column) within the space between the cathode and anode where the electrical properties (voltage, charge density, luminosity) vary along the length of the glow discharge [46,47]. Spatial variability of surface treatment can occur depending on the plasma configuration and object geometry being treated. We employed an inductively coupled RFGD plasma system composed of a helical coil configuration wrapped around a cylindrical vacuum chamber. This arrangement produces a multidirectional isotropic plasma exposure and thus the 3-dimensional surface geometry of the treated object is not a significant factor [43]. As a result, RFGD creates a more spatially uniform surface exposure to the energetic particles it generates compared to DC current plasmas. Therefore, although

our results suggest that RFGD pretreatment can alter the net charge of the surface oxide, RFGD's effects on the oxide may not be reproduced using DC-generated plasma by virtue of the differences in physics between DC glow discharge and RFGD.

Differences between our RFGD procedure and other methods using GDP [44,48] in their effects on oxide surface properties may also be attributable to the use of different gases employed to create the plasma (oxygen vs. argon, respectively). A number of considerations suggest that argon and oxygen plasmas may have very different surface physico-chemical effects on metallic implant materials that can affect their biological properties For example, Doundoulakis [49] observed that argon sputtering etched or removed portions of the titanium surface oxide, thereby altering its topography. In contrast, a plasma created from oxygen, which has a much lower atomic weight than argon, has been shown to have a smoothing effect on metal oxides believed to be due to the apposition of a thin oxide layer [50]. This latter finding confirms our observations that RFGD did not increase Ti6Al4V surface roughness or alter topography. Furthermore, the intensities of the metallic Ti and Al peaks were less in our RFGD samples compared to the controls, suggesting that oxygen plasma treatment did increase the oxide layer, an effect that cannot be reproduced with argon plasmas. Pure titanium films exposed to oxygen plasma also demonstrate a reduction in metallic titanium and have an increase in TiO_2 [51]. A similar effect may occur on titanium alloys. Therefore, the gas used to create RF or DC plasmas is an important variable in their effects on the properties of the oxide.

4.2 Mechanisms for surface charge alteration

Our study is the first to directly measure the effects of RFGD treatment on the net charge of a titanium alloy's surface oxide layer by AFM. Employing AFM, we determined that both the RFGD and heat pretreatments made the surface oxide of Ti6Al4V more negatively charged when measured at a pH of 6 or higher. However, the RFGD treated alloy samples had a higher positive net surface charge at acidic pH (pH 3–5) and a higher negative net surface charge at alkaline pH (pH 7–8.4) compared to either the heat-treated or control or samples. It is clear that either treatment induced a sustainable alteration of the alloy surface charge at the atomic level. As discussed in our earlier study, local metal oxide charge can be influenced by the acid-base balance of metal hydroxo-complexes [25]. The hydroxo-complexes of multivalent metal cations are amphoteric, exhibiting both acidic and basic properties:

$$\mathrm{M{-}OH{+}H_2O \Rightarrow [M{-}O]^- {+} H_3O^+ \ \ (acidic\ reaction)}$$
$$\mathrm{M{-}OH{+}H_2O \Rightarrow [M{-}OH_2]^+ {+} OH^- \ \ (basic\ reaction)}$$

Each metal is likely to have a unique isoelectric point, the pH at which there is an equal proportion of $[M — O]^-$ and $[M — OH_2]^+$ groups and there are no umcompensated charges. The increase in the negative net surface charge (measured at alkaline pH) promoted by heat treatment of Ti6Al4V might be related to the alloy's specific metallic composition, for two reasons. Firstly, the heating of alumina surfaces has been shown to enhance the acidity of the surface Al-OH groups to promote their deprotonation, especially at high calcination temperatures [52]. Secondly, the heat treatment-induced increase in the Al/Ti ratio in the surface oxide layer may increase the overall concentration of $M — O^-$ anions since Al-OH has an isoelectric point at a much lower pH than Ti-OH [53]. In fact, we found that heat treatment shifted the surface isoelectric point of the titanium alloy from approximately pH 6.7 to 5.4. It should be noted that the effects of heat treatment on net surface charge were both qualitatively and quantitatively different from those of RFGD, since only the latter treatment altered net surface charge at acidic pH. These findings suggest that the two treatments alter surface oxide charge via different mechanisms.

The most straightforward mechanism for the effects of RFGD treatment on oxide charge may be an increase the surface concentration of acidic M — OH groups that are likely to be deprotonated at alkaline pH or lead to the formation of. $[M — OH_2]^+$ groups at acidic pH. This explanation is supported by reports that RFGD treatment may increases the number of surface metal hydroxyl groups [22,25,26]. Additional factors may be involved in the effects of RFGD treatment on the metal oxide surface charge. As discussed previously, the RF plasma is composed of a myriad of chemical species, including electrons, reactive monoatomic cations and anions, and free radicals [42]. Some of these species produced in RF plasmas can collide with or become implanted onto the substrate, thereby producing ionization or bond rearrangements in surface atoms that may lead to changes in net surface charge. For example, optical emission spectroscopy and Langmuir probe techniques of RFGD argon/oxygen mixtures have shown the existence of oxygen radicals and O^- negative ions created within the plasma or substrate surface [53]. In addition, Olthoff and coworkers [54–55] found the presence of O_2^+ and less abundant O^+ ions in Argon/Oxygen plasma mixtures. It has been suggested that O_2 plasma treatment could promote the oxidation of surface oxygen [56], possibly leading to the formation of neutral M — O• free radicals (from deprotonated M — O^- groups) and an increase in the net positive surface charge. In any case, the effects of heat and RFGD on the relative surface concentrations of basic and acidic metal hydroxides will be determined by ESCA in a future study to clarify the physico-chemical mechanism(s) of the RFGD treatment.

Atomic force measurements made in nitrate buffer compared to the unbuffered (pure water) condition suggest that surface charge was influenced to some degree by the adsorption of counter-ions, which has been proposed as a mechanism of charge regulation for Si_3N_4 surfaces [40].. For example, control samples were found to have a net positive surface charge between pH 5 and 6.4 in nitrate buffer but exhibited no net surface charge when measurements were made at pH 5.6 in water. These findings suggest that when the control oxide surface, which is nominally neutral at pH 5.6 in water, is placed in nitrate buffer (at pH 5–6.4), the binding of Na+ ions to M — O^- groups dominates the binding of nitrate anions to $[M — OH_2]^+$ groups. thereby contributing to a net positive surface charge. However, findings that either treatment created a *negative* net surface charge in buffer between pH 5 and 6.4 suggests that the M-OH redox balance, not counter-ion binding, is the predominant surface charging mechanism for the treated samples. The mechanism for charge regulation will be further examined using atomic force measurements by altering the ionic strength of the buffer in future studies.

4.3 Effect of surface treatments on hydrophilicity

The physico-chemical mechanism(s) through which surface treatments modify the hydrophilicity of Ti6Al4V also remains to be addressed. A mechanistic explanation for the effects of heat treatment on the wettablity of the Ti6Al4V alloy might involve a simple increase in the surface concentration of M-OH groups that can participate in hydrogen bonding [57] as a result of the oxidative treatment. It is the hydrogen bonding of water to surface functional groups that exerts the greatest influence on wettability [58,59]. Since our heat treatment increased the surface concentrations of both AlOx and VOx, it might also be argued that the observed increase in hydrophilicity promoted by heating Ti6Al4V samples is partially due to oxide compositional changes [60,61]. However, when sessile drop contact angle measures were performed on commercial pure titanium (grade 2) and titanium alloy (Ti6Al4V) using water, formamide, and diiodanethane, there was no significant difference in wettability for all the test liquids [60]. Therefore, it would appear that the observed difference in wettability between control and heat-treated samples is predominantly due to factors other than changes in the oxide's elemental composition.

The effects of heat treatment on the topography and roughness of the Ti6Al4V oxide may be involved in the observed increases in hydrophilicity. Surface roughness has been demonstrated

to decrease the water contact angle of a hydrophilic surface (contact angle less than 45°) [57, 62,63]. We have previously reported that heating increased the surface roughness through oxide growth on a highly polished control sample [13].. Since, in the current study, we determined that the net surface charge of the heat and polished control samples were the same, this would suggest that roughness plays a significant role in the wettability of the heat-treated samples. Furthermore, it has been [64] reported that anodically oxidized Ti6Al4V exhibits a hydrophilic porous oxide. We observed that heating Ti6Al4V metal forms an intricate lattice of nano–elevations of the surface oxide. This morphology would increase the oxide's porosity and thus would help to explain the observed increase in wettability.

Wettability was also greatly enhanced after RF oxygen plasma treatment although the mechanism(s) may be different from those discussed above for heat treatment. One mechanism may involve an increase in surface hydroxyl functionalities [22,25–26] Alternatively, it has been suggested that the increased wettability observed after O_2 plasma treatment is due to the oxidation of surface oxygen forming a neutral O• [56]. Combining two neutral radicals produces resultant oxygen vacancies within the oxide [56] that favor the adsorption of water on the TiO_2 film. Therefore, especially since we have shown that the RFGD treatment of highly polished control Ti6Al4V samples did not increase surface roughness or alter topography, it is likely that RFGD increases wettability purely through direct effects on the chemistry of the surface oxide.

4.4 Conclusions

In this study, we have demonstrated that RFGD and heat treatment of a titanium alloy have very different effects on the surface oxide. Heat treatment increased the oxide's hydrophilicity and negative net charge and altered oxide atomic composition and topography. In contrast, RFGD treatment increased the hydrophilicity and negative net charge of the oxide without altering its surface physical structure or atomic composition. In conclusion, RFGD treatment of metallic implant materials may be used to study the role of oxide surface charge, independently of other oxide properties, in surface biomimetic protein activity and cellular osteogenesis, as demonstrated in our companion article [15].

Acknowledgments

The project described was supported by Grant Number NIH RO1 DE017695 (Awarded to DEM). The sponsor did not have any role in the study design; the collection, analysis and interpretation of data; the writing of the report; or the decision to submit the paper for publication. This material is also the result of work supported with resources and the use of facilities at the James J. Peters VA Medical Center, Bronx, New York. We would like to acknowledge Michael Stranick of Colgate Palmolive, Inc. for assistance with the ESCA measurements. Special thanks goes to Ryan Jeong and Dana McCloskey for their help in preparing and treating the alloy disks.

References

1. Larsson G, Thomsen P, Aronsson BO, Rodhal M, Lausmaa J, Kasemo B, et al. Bone response to surface-modified titanium implants: Studies on the early tissue response to machined and electropolished implants with different oxide thicknesses. Biomaterials 1996;17:605–16. [PubMed: 8652779]
2. Tengvall P, Lundström I. Physico-chemical considerations of titanium as a biomaterial. Clin Mater 1992;9:115–34. [PubMed: 10171197]
3. Morris HF, Winkler S, Ochi S. A 48-month multicenter clinical investigation: implant design and survival. J Oral Implantol 2001;27:180–86. [PubMed: 12500876]
4. Garino, J. Etiology of failure, Revis. In: Steinberg, M., editor. Total Hip Arthroplasty. Lippincott-Williams & Wilkins; New York, NY: 1999. p. 1-10.
5. Herberts, P. Revis. hip surg. In: Galante, J., editor. Total Hip Revis Surg. Raven Press; New York, NY: 1995. p. 1-17.

6. Adell R, Eriksen B, Lekholm U, Brånemark PI, Jemt T. A long-term follow-up study of osseointegrated implants in the treatment of totally edentulous jaws. Int J Oral Maxillofac Implants 1990;5:347–359. [PubMed: 2094653]
7. Adell R, Likholm U, Rockler B, Brånemark PI. A 15-year study of osseointegrated implants in the treatment of the edentulous jaw. Int J Oral Surg 1981;10:387–416. [PubMed: 6809663]
8. Hardt CR, Grondahl K, Lekholm U, Wennstrom JL. Outcome of implant therapy in relation to experienced loss of periodontal bone support: A retrospective 5-year study. Clin Oral Implants Res 2002;13:488–94. [PubMed: 12453125]
9. Johansson P, Strid KG. Assessment of bone quality from cutting resistance during i mplant surgery. Int J Oral Maxillofac Implants 1994;9:279–288.
10. Anselme K, Linez P, Bigerelle M, Le Maguer D, Le Maguer A, Hardouin P, et al. The relative influence of the topography and chemistry of TiAl6V4 surfaces on osteoblastic cell behavior. Biomater 2002;21:1567–77.
11. Kieswetter K, Schwartz Z, Hummert TW, Cochran DL, Simpson J, Dean DD, et al. Surface roughness modulates the local production of growth factors and cytokines by osteoblast-like MG-63 cells. J Biomed Mater Res 1996;32:55–63. [PubMed: 8864873]
12. MacDonald DE, Deo N, Markovic B, Stranick M, Somasundaran P. Adsorption and dissolution behavior of human plasma fibronectin on heatly and chemically modified titanium dioxide particles. Biomaterials 2002;23:1269–1279. [PubMed: 11791930]
13. MacDonald DE, Rapuano BE, Deo N, Stranick M, Boskey AL, Somasundaran P. Heat and chemical modification of titanium-aluminum-vanadium implant materials: effects on surface properties, glycoprotein adsorption, and MG63 cell attachment. Biomaterials 2004;25:3135–3146. [PubMed: 14980408]
14. Martin JY, Schwartz Z, Hummert TW, Schraub DM, Simpson J, Lankford J, et al. Effect of titanium surface roughness on proliferation, differentiation, and protein synthesis of human osteoblast-like cells (MG63). J Biomed Mater Res 1995;29:389–401. [PubMed: 7542245]
15. Rapuano BE, MacDonald DE. Surface oxide charge/hydrophilicity of a titanium alloy: modulation of fibronectin-activated attachment and spreading of osteogenic cells. 2010 Submitted Colloids Surf., B.
16. Kasemo B, Lausmaa J. Surface science aspects of inorganic biomaterials. CRC Crit Rev Biocompat 1986;2:335–380.
17. Ratner BD, Castner DG, Horbett TA, Lenk TJ, Lewis KB, Rapoza RJ. Biomolecules and surfaces. J Vac Sci Technol A 1990;8:2306–17.
18. Milosev I, Metikos-Hukovic M, Stehblow HH. Passive film on orthopaedic TiAlV alloy formed in physiological solution investigated by X-ray photoelectron spectroscopy. Biomaterials 2000;21:2103–13. [PubMed: 10966021]
19. Baier RE, Meyer AE, Natiella JR, Carter JM. Surface properties determine bioadhesive outcomes: methods and results. J Biomed Mater Res 1984;18:337–45.
20. Aronsson BO, Lausmaa J, Kasemo B. Glow discharge plasma treatment for surface cleaning and modification of metallic biomaterials. J Biomed Mater Res 1997;35:49–73. [PubMed: 9104698]
21. Shibata Y, Hosaka M, Kawai H, Miyazaki T. Glow discharge plasma treatment of titanium plates enhances adhesion of osteoblast-like cells to the plates through the integrin-mediated mechanism. Int J Oral Maxillofac Implants 2002;17:771–777. [PubMed: 12507235]
22. Kim YJ, Kang IK, Huh MW, Yoon SC. Surface characterization and in vitro blood compatibility of poly(ethylene terephthalate) immobilized with insulin and/or heparin using plasma glow discharge. Biomaterials 2000;21:121–130. [PubMed: 10632394]
23. Triolo PM, Andrade JD. Surface modification and characterization of some commonly used catheter materials. II. Friction characterization. J Biomed Mater Res 1983;17:149–165. [PubMed: 6826571]
24. Golander CG, Pitt WG. Characterization of hydrophobicity gradients prepared by means of radio frequency plasma discharge. Biomaterials 1990;11:32–5. [PubMed: 2302447]
25. Vargo TG, Bekos EJ, Kim YS, Ranieri JP, Bellamkonda R, Aebischer P, Margevich DE, Thompson PM, Bright FV, Gardella JA Jr. Synthesis and characterization of fluoropolymeric substrata with immobilized minimal peptide sequences for cell adhesion studies. I J Biomed Mater Res 1995;29:767–78.

26. Ozden N, Ayhan H, Erkut S, Can G, Piskin E. Coating of silicone-based impression materials in a glow-discharge system by acrylic acid plasma. Dent Mater 1997;13:174–8. [PubMed: 9758971]
27. Parks GA. The isoelectric points of solid oxides, solid hydroxides, and aqueous hydroxo complex systems. Chem Rev 1965;65:177–198.
28. Annual book of ASTM standards. Vol. 13.01. Amer. Soc. for Test. and Mater; USA: 1996. F-86 AS, Standard practice for surface preparation and marking of metallical surgical implants; p. 6-8.
29. Parr GR, Gradner LK, Toth RW. Titanium: the mystery metal of implant dentistry. Dental materials aspects. J Prosthet Dent 1985;54:410–4. [PubMed: 3864976]
30. MacDonald DE, Markovic B, Allen M, Somasundaran P, Boskey AL. Surface analysis of human plasma fibronectin adsorbed to commercially pure titanium materials. J Biomed Mater Res 1998;41:120–30. [PubMed: 9641632]
31. Cappella B, Dietler G. Force–distance curves by atomic force microscopy. Surf Sci Rep 1999;34:1–104.
32. Kilpadi DV, Raikar GN, Liu J, Lemons JE, Vohra Y, Gregory JC. Effect of surface treatment on unalloyed titanium implants: Spectroscopic analyses. J Biomed Mater Res 1998;40:646–59. [PubMed: 9599042]
33. Schwartz A, Raz P, Zhao G, Barak Y, Tauber M, Yao H, Boyan BD. Effect of micrometer-scale roughness of the surface of Ti6Al4V pedicle screws in vitro and in vivo. J Bone Joint Surg Am 2008;90:2485–98. [PubMed: 18978418]
34. Sodhi RNS, Weninger A, Davies JE, Sreenivas K. X-ray photoelectron spectroscopic comparison of sputtered Ti, Ti6Al4V, and passivated bulk metals for use in cell culture techniques. J Vac Sci Technol A 1991;9:1329–33.
35. Pham MT, Zyganow I, Matz W, et al. Corrosion behavior and microstructure of titanium implanted with α and β stabilizing elements. Thin Solid Films 1997;310:251–59.
36. Okazaki Y, Tateishi T, Ito Y. Corrosion resistance of implant alloys in pseudo physiological solution and role of alloying elements in passive films. Mater Trans JIM 1997;38:78–84.
37. Rao CNR, Sarma DD, Vasudevan S, Hegde MS. Study of transition metal oxides by photoelectron spectroscopy. Proc R Soc London 1979;67:239–52.
38. Moulder, JF.; Stickel, WF.; Sobol, PE.; Bomben, KD. Physic Electron Corp. Eden Prairie; MN: 1992. Handbook of Photoelect. Spectrosc.
39. Mezzasalma SA. Effect of Mixing Entropy on the Static Yield Stress of a Liquid Dispersion of Solid Particles: Comparison between Si3 N4 and Ca3 (PO4)2 Aqueous Suspensions. J Colloids Interface Sci 1997;190:302–306.
40. Senden TJ, Drummond CJ. Surface chemistry and tipsample interaction in atomic force microscopy. Colloids Surf, A 1995;94:29–51.
41. Hartley PG, Larson L, Scales PJ. Electrokinetic and direct force measurements between silica and mica surfaces in dilute electrolyte solutions. Langmuir 1997;13:2207–2214.
42. Hopwood J. Review of inductively coupled plasmas for plasma processing. Plasma Sources Sci Technol 1992;1:109–116.
43. Swart KM, Keller JC, Wightman JP, Draughn RA, Stanford CM. Short-term plasma-cleaning treatments enhance *in vitro* osteoblastic attachment to titanium. J Oral Implantol 1992;18:130–137. [PubMed: 1289550]
44. Shibata Y, Hosaka M, Kawai H, Miyazaki T. Glow discharge plasma treatment of titanium plates enhances adhesion of osteoblast-like cells to the plates through the integrin-mediated mechanism. Int J Oral Maxillofac Implants 2002;17:771–777. [PubMed: 12507235]
45. Aronsson BO, Lausmaa J, Kasemo B. Glow discharge plasma treatment for surface cleaning and modification of metallic biomaterials. J Biomed Mater Res 1997;35:49–73. [PubMed: 9104698]
46. Roth, JR. Industr plasma Engineering v1: principles. Instit. of Physics Publishing; Bristol, UK: 1995.
47. Chapman, B. Glow Discharge processes: Sputtering and Plasma Etching. Wiley-Interscience Publications; New York: 1980.
48. Yamamoto H, Shibata Y, Miyazaki T. Anode glow discharge plasma treatment of titanium plates facilitates adsorption of extracellular matrix proteins. J Dent Res 2005;84:668–671. [PubMed: 15972599]

49. Doundoulakis JH. Surface analysis of titanium after sterilization: Role in implant-tissue interface and bioadhesion. J Prosthet Dent 1987;56:471–478. [PubMed: 3478480]
50. Li Z, Beck P, Douglas AA, Ohlberg AA, Stewart DR, Williams RS. Surface properties of platinum thin films as a function of plasma treatment conditions. Surf Sci 2003;529:410–418.
51. Rossetti FF, Reviakine I, Textor M. Characterization of titanium oxide films prepared by the template-stripping method. Langmuir 2003;19:10116–10123.
52. Deng F, Wang G, Du Y, Ye C, Kong Y, Li X. 1H MAS and 1H[23Na] double resonance NMR studies on the modification of surface hydroxyl groups of gamma-alumina by sodium. Solid State Nucl Magn Reson 1997;7:281–90. [PubMed: 9176933]
53. Pavlík J, Hrach R, Hedbávný P, Šovíèek P. Study of argon/oxygen plasma used for creation of aluminium oxide thin films. Superficies y Vacio 1999;9:131–134.
54. Olthoff JK, Van Brunt RJ, Radovanov SB. Effect of electrode material on measured ion energy distributions in radio-frequency discharges. Appl Phys Lett 1995;67:473–475.
55. Olthoff JK, Van Brunt RJ, Radovanov SB. Studies of ion kinetic-energy distributions in the gaseous electronics conference RF reference cell. J of Res of the Nat Instit of Stand and Technol 1995;100:383–400.
56. Han JB, Wang X, Wang N, Wei ZH, Yu GP, Zhou ZG, Wang QQ. Effect of plasma treatment on hydrophilic properties of TiO_2 thin films. Surf & Coat Technol 2006;200:4876–4878.
57. Jennissen HP. Ultra-hydrophile metallische biomaterialien. Biomaterialien 2001;2:45–53.
58. Vogler, EA. Interf chemin biomater Sci. Berg, J., editor. Wettability, Marcel Dekker; New York: 1993k. p. 184-250.
59. Vogler EA. Structure and reactivity of water at biomaterial surfaces. Adv Colloids Interface Sci 1998;74:69–117.
60. Woodward JT, Gwin H, Schwartz DK. Contact angles on surfaces with mesoscopic chemical heterogeneity. Langmuir 2000;16:2957–2961.
61. Sun T, Song W, Jiang L. Control over the responsive wettability of poly(N-isopropylamide0 film in a large extent by introducing an irresponsive molecule. Chem Commun 2005;13:1723–1725.
62. Adamson, AW. Phys Chem of Surf. John Wiley & Sons, Inc; New York: 1990. p. 399
63. Lim LJ, Oshida Y. Initial contact angle measurements on variously treated dental/medical titanium materials. Biomed Mater and Engineering 2001;11:325–341.
64. Zwilling V, Darque-Ceretti E, Boutry-Forveille A, David D, Perrin MY, Aucouturier M. Structure and physicochemistry of anodic oxide films on titanium and TA6V alloy. Surf Interface Anal 1999;27:629–637.

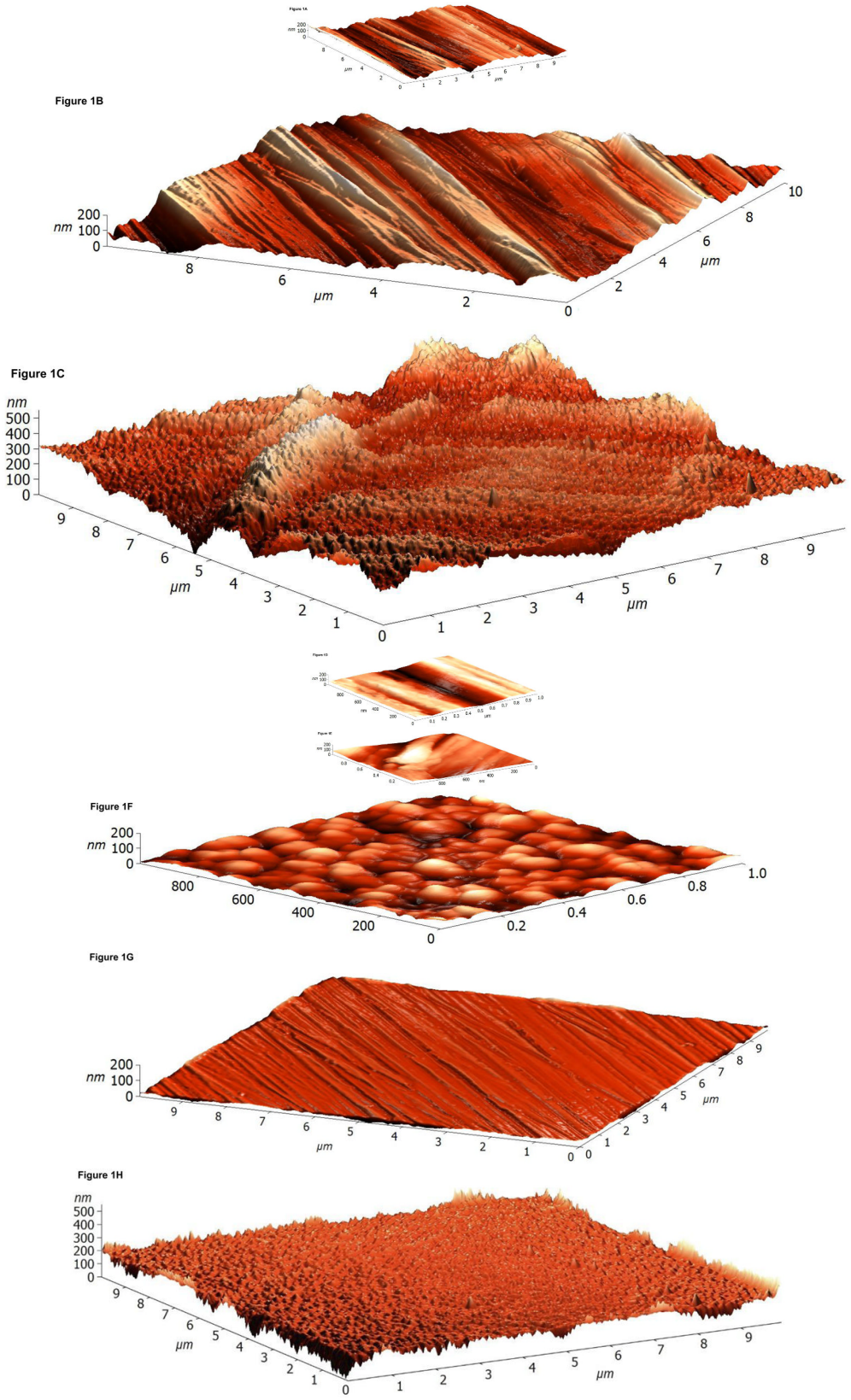

Fig. 1.

Atomic Force Microscopy (AFM) images of (A,D) control, (B,E) RFGD-treated and (C,F) heat- treated Ti-6Al-4V samples for a (A-C) 10 × 10 μm scan area or a (D-F) 1 × 1 μm scan area. After applying a spatial high-pass filtering with a 200 nm cutoff to figures 1B and 1C, respectively, only the small-scale features of the RFGD-treated (G) and (H) heat treated samples remain.

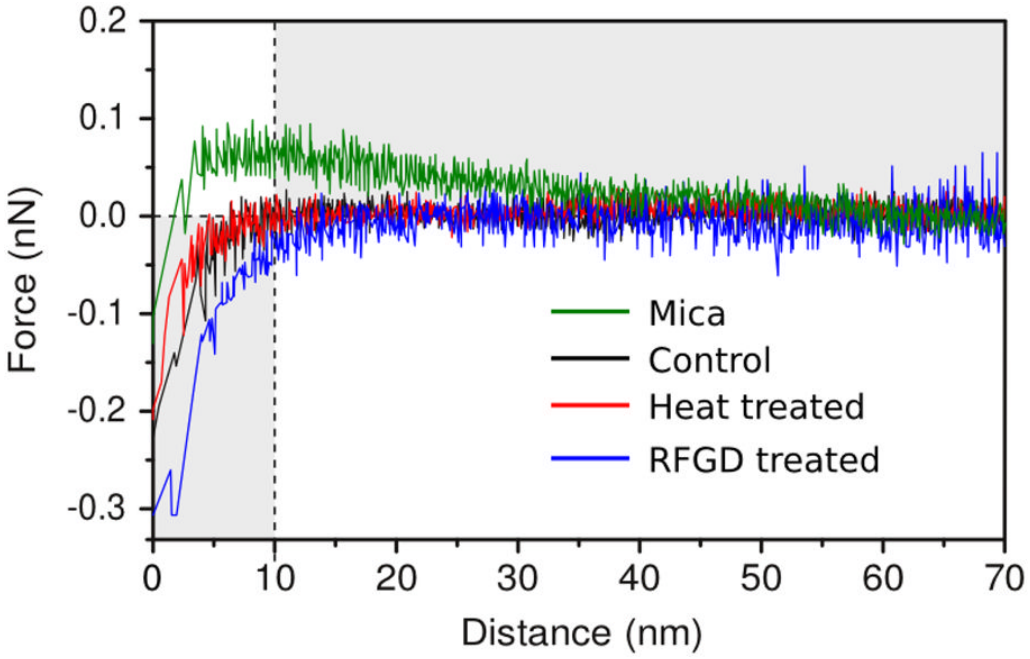

Fig. 2.

Forces between a negatively charged silicon nitride AFM probe and control, heat-treated and RFGD-treated Ti6Al4V samples or a mica surface in water. Atomic forces of attraction or repulsion were measured for control and treated surfaces in picopure water at pH 5.6. The Z distance decreases as the sample surface is brought closer to the silicon nitride tip. Long-range electrostatic forces are measured at Z distances greater than 10 nm whereas interactions between 0–10 nm are dominated by van der Waals forces. A force of repulsion upon approach is signified by an increase in the size of the deflection of the tip compared to baseline deflection. A force of attraction is signified by a decrease in the size of the deflection of the tip compared to baseline deflection. Three disks were analyzed for each experimental group. The data obtained for each individual metal disk represent an average of 30–40 force curves acquired at 15 different sample locations for each disk. The three averaged force curves obtained for the disks in each experimental group were then averaged to obtain the final force curves presented in the figure.

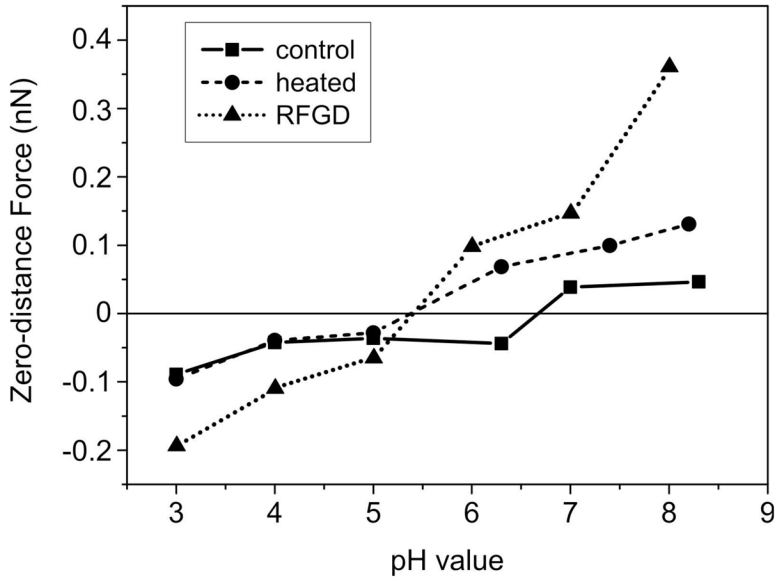

Fig. 3.

Forces between a negatively charged silicon nitride AFM probe and control, heat-treated and RFGD-treated Ti6Al4V samples or a mica surface in a nitrate buffer. Atomic forces of attraction or repulsion were measured for control and treated surfaces in 2 mM sodium nitrate buffer at a range of pH's between 3 and 8.4. Exponential decay curves $f(z) = b \cdot \exp[-az]$ were fitted to model the electrostatic double layer forces. The fit parameters a and b represent the Debye length and the electrostatic force at zero distance, respectively. The mean electrostatic zero-distance force at each pH is presented as a measure of the strength of the electrostatic interaction between the tip and the surface. A total of three control and treatment disks were analyzed. The data obtained for each individual metal disk analyzed represents an average of five random sample locations per disk at each pH value and 10 force curves performed at each site. The three averaged values obtained for the disks in each experimental group at each pH shown were then averaged to obtain the final data points presented in the figure.

Table 1

Calculated RMS roughness values of the AFM topography images of control and processed allow substrates after spatial high-pass filtering (cutoff 200 nm).

	RMS roughness of sub-200 nm features
Control	4.1 ± 1.1 nm
Heat-treated	12.8 ± 1.7 nm
RFGD-treated	3.6 ± 0.9 nm

[a] Values are mean of at least 3 samples for each treatment (mean ± standard deviation).

Table 2

Surface Composition as Determined by ESCA

Sample	Atomic Percent					Atomic Ratio		
	C	O	Ti	Al	V	Al/Ti	V/Ti	V/Al
Polished	21.96	50.00	23.95	3.59	0.50	0.15	0.021	0.14
RFGD	21.04	51.72	23.26	3.41	0.58	0.15	0.025	0.17
600C	24.13	49.48	13.10	8.52	4.78	0.65	0.37	0.57

- data are reproducible to ± 12% rsd or better

- N was also detected on all samples at below 0.6 at. %

Table 3

Wettability measurements for titanium-aluminum-vanadium samples following modification by thermal or RFGD treatment[a]

Ti6Al4V treatment	Contact Angle (°)
Control	43.0 ± 5.3
Heated (600 C)	16.0 ± 2.0*
RFGD	17.3 ± 6.0*

[a] Values are mean of at least 10 samples for each treatment (mean ± standard deviation).

* Significantly different from control based on ANOVA ($p < 0.001$)